

On the accuracy of the melting curves
drawn from modelling a solid as an elastic medium

Santi Prestipino [*]

Università degli Studi di Messina, Dipartimento di Fisica,

Contrada Papardo, I-98166 Messina, Italy

(Dated: September 24, 2018)

Abstract

An ongoing problem in the study of a classical many-body system is the characterization of its equilibrium behaviour by theory or numerical simulation. For purely repulsive particles, locating the melting line in the pressure-temperature plane can be especially hard if the interparticle potential has a softened core or contains some adjustable parameters. A method is hereby presented that yields reliable melting-curve topologies with negligible computational effort. It is obtained by combining the Lindemann melting criterion with a description of the solid phase as an elastic continuum. A number of examples are given in order to illustrate the scope of the method and possible shortcomings. For a two-body repulsion of Gaussian shape, the outcome of the present approach compares favourably with the more accurate but also more computationally demanding self-consistent harmonic approximation.

Keywords: Empirical melting rules, linear elasticity, self-consistent harmonic approximation

I. INTRODUCTION

There exists as yet no comprehensive theoretical treatment of the solid-liquid phase transition that can rival in quality and accuracy the smooth-cutoff formulation of the hierarchical reference theory of the liquid-vapour transition [2], which yields flat pressure vs. density isotherms in the coexistence region as well as distinct binodal and spinodal curves. Most theoretical and simulational strategies for detecting a point of solid-liquid coexistence invariably pass through the prior determination of the (Gibbs-) free energy for the two separate phases. Theoretical approaches include classical density-functional theories and thermodynamic perturbation theory [3]. In Monte Carlo simulations, the Frenkel-Ladd method and the Widom particle-insertion method may be employed, in conjunction with thermodynamic integration, in order to obtain accurate solid and liquid chemical potentials in the transition region [4]. On the far opposite side, lie a by now considerable number of empirical one-phase melting and freezing criteria which allow a rough estimate of the limit of stability for the given solid or liquid phase. Familiar examples are the Lindemann melting rule and the Hansen-Verlet freezing criterion, both relying on quantities that are computed numerically (the mean square displacement in the solid and the structure factor in the liquid).

I hereby consider a semi-empirical method for the melting transition which, rather than being meant as a rule to provide a reliable estimate of the upper stability threshold of a solid with prescribed symmetry, is actually aimed at anticipating with little effort (*i.e.*, without resorting to numerical simulation) at least the topology of the transition line, which may be useful especially in those cases where multiple solid phases and/or reentrant-fluid anomalies are expected [5]. Assuming two-body forces between the particles, the idea is to treat the solid system as an elastic medium whose pressure-dependent moduli are determined at zero temperature from the potential. The upper limit of thermodynamic stability of the solid is then taken in accordance with the Lindemann rule [6]. Aside from the approximate character of the Lindemann criterion, the main error in the estimate of the melting temperature $T_m(P)$ comes partly from neglecting all anharmonicities in the particle dynamics and partly from assuming the same elastic moduli at all temperatures. Both sources of approximation are expected to extend solid stability well beyond the actual threshold. In spite of this, the *shape* of $T_m(P)$ is reasonably well reproduced by this criterion, as I shall demonstrate for a number of model potentials (exceptions are anyway encountered – see below).

After a reminder of elasticity theory in Section 2, I introduce the novel criterion of melting in Section 3 along with a few applications. In Section 4, I compare the indication of (what might be called) the elastic criterion of melting for the repulsive Gaussian potential with the outcomes of more refined approaches, based on the theory of the harmonic crystal and on the self-consistent harmonic approximation. Conclusions are postponed to Section 5.

II. A BRIEF ACCOUNT OF LINEAR ELASTICITY

The information gathered here is standard reference material which is preparatory to the theoretical analysis that will be outlined in the next Section [8].

Consider the Bravais lattice $\{\mathbf{R}_n\}$ of a crystal with $N \gg 1$ atoms (classical point particles) and let $\mathbf{x}_n = \mathbf{R}_n + \mathbf{u}(\mathbf{R}_n)$ be the actual position of the n -th atom (to simplify the notation, I choose $\mathbf{R}_1 = 0$ in the following). In the simplest terms, the basic equations of linear elasticity stem from evaluating the total potential energy U of the crystal in the approximation where $\mathbf{u}(\mathbf{R}) - \mathbf{u}(\mathbf{R}')$ is expanded to linear order in $\mathbf{R} - \mathbf{R}'$. For a homogeneous deformation, this amounts to replacing $x_{n\alpha}$ with

$$R_{n\alpha} + \sum_{\beta=1}^3 u_{\alpha\beta} R_{n\beta} \quad (2.1)$$

for $\alpha = 1, 2, 3$, $u_{\alpha\beta}$ being a constant. If the continuum limit is taken, we can think of $u_{\alpha\beta}$ as just the constant value of $\partial u_\alpha / \partial x_\beta$. Concurrently, the deformation also modifies the crystal volume from V_0 to V :

$$\frac{V}{V_0} = \det(\delta_{\alpha\beta} + u_{\alpha\beta}) = 1 + \sum_{\alpha} e_{\alpha\alpha} + \frac{1}{2} \sum_{\alpha,\beta} (e_{\alpha\alpha} e_{\beta\beta} - e_{\alpha\beta}^2) + \frac{1}{2} \sum_{\alpha,\beta} \omega_{\alpha\beta}^2, \quad (2.2)$$

where third-order terms in the strains were neglected. In Eq. (2.2),

$$e_{\alpha\beta} = \frac{1}{2}(u_{\alpha\beta} + u_{\beta\alpha}) \quad (2.3)$$

is the *strain tensor* while $\omega_{\alpha\beta} = (u_{\alpha\beta} - u_{\beta\alpha})/2$. Our objective is to evaluate U up to second order in the $u_{\alpha\beta}$. Assuming a smooth spherically-symmetric pair potential $\phi(r)$ and specializing the analysis to crystals of cubic symmetry, a straightforward but tedious derivation yields:

$$\begin{aligned} u \equiv \frac{U}{N} &= \frac{1}{2} \sum_{n=2}^N \phi(|\mathbf{x}_n|) = u_0 - P(v - v_0) + \frac{1}{2} v_0 \lambda_1 (e_{xx}^2 + e_{yy}^2 + e_{zz}^2) \\ &+ v_0 \lambda_2 (e_{xx} e_{yy} + e_{xx} e_{zz} + e_{yy} e_{zz}) + 2v_0 \lambda_3 (e_{xy}^2 + e_{xz}^2 + e_{yz}^2), \end{aligned} \quad (2.4)$$

with $v_0 = V_0/N$, $u_0 = (1/2) \sum_{n=2}^N \phi(|\mathbf{R}_n|)$, and

$$P = -\frac{1}{6v_0} \sum_{n=2}^N |\mathbf{R}_n| \phi'(|\mathbf{R}_n|). \quad (2.5)$$

Moreover, three *elastic constants* (or Lamé coefficients) appear in Eq. (2.4):

$$\begin{aligned} \lambda_1 &= -P + \frac{1}{2v_0} \sum_{n=2}^N \frac{X_n^4}{|\mathbf{R}_n|^4} [|\mathbf{R}_n|^2 \phi''(|\mathbf{R}_n|) - |\mathbf{R}_n| \phi'(|\mathbf{R}_n|)] ; \\ \lambda_2 &= P + \frac{1}{2v_0} \sum_{n=2}^N \frac{X_n^2 Y_n^2}{|\mathbf{R}_n|^4} [|\mathbf{R}_n|^2 \phi''(|\mathbf{R}_n|) - |\mathbf{R}_n| \phi'(|\mathbf{R}_n|)] ; \\ \lambda_3 &= \lambda_2 - 2P, \end{aligned} \quad (2.6)$$

where X_n, Y_n , and Z_n are the Cartesian components of \mathbf{R}_n . The three λ 's are the same quantities which are more commonly denoted c_{11}, c_{12} , and c_{44} , respectively. In Eq. (2.4), the term linear in the $u_{\alpha\beta}$ and actually proportional to the trace of the strain tensor corresponds to the stress due to an applied pressure P . Equation (2.5) links the lattice parameter (or the crystal volume V_0) with the pressure. The identification of P with the system pressure ensures consistency of Eq. (2.4) with the thermodynamic definition of pressure.

A more general form of Eq. (2.4), valid for any temperature T , is the following:

$$g = g_0 + \frac{1}{2} v_0 \sum_{\alpha, \beta, \gamma, \delta} c_{\alpha\beta\gamma\delta} e_{\alpha\beta} e_{\gamma\delta}, \quad (2.7)$$

where g is the Gibbs free energy per particle. Equation (2.7) reduces to (2.4) for $T = 0$ and a crystal in the cubic system. The maximum number of independent elastic constants $c_{\alpha\beta\gamma\delta}$ is 21 (taking Voigt symmetry into account), in fact they reduce to just three for crystals of cubic symmetry, five for crystals of hexagonal symmetry, and so on. For instance, for hexagonal solids Eq. (2.7) takes the form

$$\begin{aligned} g &= g_0 + 2v_0 \lambda_1 (e_{xx} + e_{yy})^2 + v_0 \lambda_2 [(e_{xx} - e_{yy})^2 + 4e_{xy}^2] \\ &+ \frac{1}{2} v_0 \lambda_3 e_{zz}^2 + 2v_0 \lambda_4 (e_{xx} + e_{yy}) e_{zz} + 4v_0 \lambda_5 (e_{xz}^2 + e_{yz}^2), \end{aligned} \quad (2.8)$$

with the following $T = 0$ values of the Lamé coefficients:

$$\begin{aligned}
\lambda_1 &= \frac{1}{12v_0} \sum_{n=2}^N \frac{X_n^4}{|\mathbf{R}_n|^4} [|\mathbf{R}_n|^2 \phi''(|\mathbf{R}_n|) - |\mathbf{R}_n| \phi'(|\mathbf{R}_n|)] ; \\
\lambda_2 &= \lambda_1 - \frac{P}{2} ; \\
\lambda_3 &= -P + \frac{1}{2v_0} \sum_{n=2}^N \frac{Z_n^4}{|\mathbf{R}_n|^4} [|\mathbf{R}_n|^2 \phi''(|\mathbf{R}_n|) - |\mathbf{R}_n| \phi'(|\mathbf{R}_n|)] ; \\
\lambda_4 &= \frac{P}{2} + \frac{1}{4v_0} \sum_{n=2}^N \frac{X_n^2 Z_n^2}{|\mathbf{R}_n|^4} [|\mathbf{R}_n|^2 \phi''(|\mathbf{R}_n|) - |\mathbf{R}_n| \phi'(|\mathbf{R}_n|)] ; \\
\lambda_5 &= \lambda_4 - P .
\end{aligned} \tag{2.9}$$

For tetragonal crystals, one similarly finds

$$\begin{aligned}
g &= g_0 + \frac{v_0}{2} [\lambda_1(e_{xx}^2 + e_{yy}^2) + 2\lambda_2 e_{xx} e_{yy} + 4\lambda_3 e_{xy}^2 \\
&\quad + \lambda_4 e_{zz}^2 + 2\lambda_5(e_{xx} + e_{yy})e_{zz} + 4\lambda_6(e_{xz}^2 + e_{yz}^2)] ,
\end{aligned} \tag{2.10}$$

with zero-temperature Lamé coefficients given by

$$\begin{aligned}
\lambda_1 &= -P + \frac{1}{2v_0} \sum_{n=2}^N \frac{X_n^4}{|\mathbf{R}_n|^4} [|\mathbf{R}_n|^2 \phi''(|\mathbf{R}_n|) - |\mathbf{R}_n| \phi'(|\mathbf{R}_n|)] ; \\
\lambda_2 &= P + \frac{1}{2v_0} \sum_{n=2}^N \frac{X_n^2 Y_n^2}{|\mathbf{R}_n|^4} [|\mathbf{R}_n|^2 \phi''(|\mathbf{R}_n|) - |\mathbf{R}_n| \phi'(|\mathbf{R}_n|)] ; \\
\lambda_3 &= \lambda_2 - 2P ; \\
\lambda_4 &= -P + \frac{1}{2v_0} \sum_{n=2}^N \frac{Z_n^4}{|\mathbf{R}_n|^4} [|\mathbf{R}_n|^2 \phi''(|\mathbf{R}_n|) - |\mathbf{R}_n| \phi'(|\mathbf{R}_n|)] ; \\
\lambda_5 &= P + \frac{1}{2v_0} \sum_{n=2}^N \frac{X_n^2 Z_n^2}{|\mathbf{R}_n|^4} [|\mathbf{R}_n|^2 \phi''(|\mathbf{R}_n|) - |\mathbf{R}_n| \phi'(|\mathbf{R}_n|)] ; \\
\lambda_6 &= \lambda_5 - 2P .
\end{aligned} \tag{2.11}$$

At $T = 0$, the expansion of the Helmholtz free energy $F = Nf$ in powers of the strain-tensor components is the same as for U . For non-zero temperatures, the respective $c_{\alpha\beta\gamma\delta}$ are instead different (one thus distinguishes isothermal and adiabatic elastic constants). For any T , the Helmholtz free energy of a solid under arbitrary initial stress can otherwise be expanded to second order in the components of the displacement gradients $u_{\alpha\beta}$,

$$\frac{f - f_0}{v_0} = \sum_{\alpha,\beta} S_{\alpha\beta} u_{\alpha\beta} + \frac{1}{2} \sum_{\alpha,\beta,\gamma,\delta} S_{\alpha\beta\gamma\delta} u_{\alpha\beta} u_{\gamma\delta} ; \tag{2.12}$$

alternatively, f can be written as a truncated power series of the Lagrangian strain parameters,

$$\eta_{\alpha\beta} = \frac{1}{2} \left(u_{\alpha\beta} + u_{\beta\alpha} + \sum_{\gamma} u_{\gamma\alpha} u_{\gamma\beta} \right), \quad (2.13)$$

with yet different coefficients in the linear and quadratic terms:

$$\frac{f - f_0}{v_0} = \sum_{\alpha,\beta} C_{\alpha\beta} \eta_{\alpha\beta} + \frac{1}{2} \sum_{\alpha,\beta,\gamma,\delta} C_{\alpha\beta\gamma\delta} \eta_{\alpha\beta} \eta_{\gamma\delta}. \quad (2.14)$$

It is then a simple exercise to show that $S_{\alpha\beta} = C_{\alpha\beta}$ and $S_{\alpha\beta\gamma\delta} = C_{\alpha\beta\gamma\delta} + C_{\beta\delta} \delta_{\alpha\gamma}$. Moreover, for $C_{\alpha\beta} = -P \delta_{\alpha\beta}$, one finds that

$$c_{\alpha\beta\gamma\delta} = C_{\alpha\beta\gamma\delta} + P(\delta_{\alpha\beta} \delta_{\gamma\delta} - \delta_{\alpha\gamma} \delta_{\beta\delta} - \delta_{\alpha\delta} \delta_{\beta\gamma}). \quad (2.15)$$

Equation (2.15) is useful for computing the λ 's at $T > 0$ through numerical simulation since specific virial-like formulae exist for the C 's [9].

An important issue is mechanical stability of a crystal phase, which is a prerequisite for its thermodynamic stability: an applied strain may destabilize the crystal, which in this case is really stable only at zero temperature. The elastic constants in Eq. (2.7) must obey so-called stability conditions in order for the unstrained crystal to resist any infinitesimal deformation, *i.e.*, in order for the crystal lattice $\{\mathbf{R}_n\}$ to provide a minimum (not just an extremum) for g . Depending on the interparticle potential and on the pressure value, the crystal may or may not be mechanically stable, meaning that it does typically exist as a stable structure for $T > 0$ only within one or more definite pressure ranges.

Using Voigt symmetry, the elastic constants of a cubic crystal can be arranged in the 6×6 matrix

$$\begin{pmatrix} \lambda_1 & \lambda_2 & \lambda_2 & | & 0 & 0 & 0 \\ \lambda_2 & \lambda_1 & \lambda_2 & | & 0 & 0 & 0 \\ \lambda_2 & \lambda_2 & \lambda_1 & | & 0 & 0 & 0 \\ \hline 0 & 0 & 0 & | & \lambda_3 & 0 & 0 \\ 0 & 0 & 0 & | & 0 & \lambda_3 & 0 \\ 0 & 0 & 0 & | & 0 & 0 & \lambda_3 \end{pmatrix} \quad (2.16)$$

and Eq. (2.7) becomes a quadratic form, $g = g_0 + (v_0/2) \sum_{a,b=1}^6 c_{ab} e_a e_b$ with $e_1 = e_{xx}$, $e_2 = e_{yy}$, $e_3 = e_{zz}$, $e_4 = 2e_{yz}$, $e_5 = 2e_{xz}$, $e_6 = 2e_{xy}$. The eigenvalues (with multiplicities) of (2.16) are λ_3 (3), $\lambda_1 - \lambda_2$ (2), and $\lambda_1 + 2\lambda_2$ (1), leading to three stability conditions:

$$\lambda_1 + 2\lambda_2 \geq 0; \quad \lambda_3 \geq 0; \quad \lambda_1 - \lambda_2 \geq 0. \quad (2.17)$$

The first two conditions amount to requiring the existence of the bulk and the shear modulus, respectively. The last inequality prescribes rigidity of the cubic solid against tetragonal shear. For a hexagonal crystal, a similar analysis yields four conditions,

$$\lambda_2 \geq 0; \lambda_5 \geq 0; 8\lambda_1 + \lambda_3 \geq 0; \lambda_1\lambda_3 - \lambda_4^2 \geq 0, \quad (2.18)$$

becoming five for tetragonal crystals:

$$\lambda_3 \geq 0; \lambda_6 \geq 0; \lambda_1 - \lambda_2 \geq 0; \lambda_1 + \lambda_2 + \lambda_4 \geq 0; \lambda_4(\lambda_1 + \lambda_2) - 2\lambda_5^2 \geq 0. \quad (2.19)$$

Tightly related to the subject of solid elasticity is the general harmonic theory of lattice dynamics. Consider a finite crystal with externally applied classical forces, and let the forces be restricted to the surface region so as to represent stresses applied to the crystal. Since the total force on each atom must vanish when the atoms are located at the equilibrium positions $\{\mathbf{R}_n\}$, the total energy at $T = 0$ can be approximately written as

$$U = U_0 + \frac{1}{2} \sum_{\mathbf{R}, \mathbf{R}'} \sum_{\alpha, \beta} \Phi_{\alpha\beta}(\mathbf{R} - \mathbf{R}') u_\alpha(\mathbf{R}) u_\beta(\mathbf{R}') \quad (2.20)$$

with $U_0 = U(\mathbf{R}_1, \dots, \mathbf{R}_N)$, all anharmonicities being neglected. The Φ coefficients in (2.20) are second-order derivatives,

$$\Phi_{\alpha\beta}(\mathbf{R} - \mathbf{R}') = \left(\frac{\partial^2 U}{\partial u_\alpha(\mathbf{R}) \partial u_\beta(\mathbf{R}')} \right)_0, \quad (2.21)$$

and, for a Bravais crystal, they are invariant under the exchange $\alpha \leftrightarrow \beta$ because of the lattice inversion symmetry. Invariance of the energy value following a rigid translation of the crystal further leads to $\sum_{\mathbf{R}} \Phi_{\alpha\beta}(\mathbf{R}) = 0$ for any α and β .

The equations of motion for the potential energy (2.20) read

$$m\ddot{u}_\alpha(\mathbf{R}) = - \sum_{\mathbf{R}', \beta} \Phi_{\alpha\beta}(\mathbf{R} - \mathbf{R}') u_\beta(\mathbf{R}'), \quad (2.22)$$

where m is the particle mass, and are solved in terms of plane waves (the *normal modes of vibration*),

$$\epsilon_\alpha(\mathbf{q}) e^{i[\mathbf{q} \cdot \mathbf{R} - \omega(\mathbf{q})t]} \quad (\alpha = 1, 2, 3). \quad (2.23)$$

The N values of \mathbf{q} lie within the first Brillouin zone (1BZ) of the lattice and are so chosen as to allow for the periodic repetition of the lattice outside its boundaries. Upon introducing the (real symmetric) *dynamical matrix*

$$B_{\alpha\beta}(\mathbf{q}) = \sum_{\mathbf{R}} \Phi_{\alpha\beta}(\mathbf{R}) e^{i\mathbf{q} \cdot \mathbf{R}} = - \sum_{\mathbf{R}} \Phi_{\alpha\beta}(\mathbf{R}) [1 - \cos(\mathbf{q} \cdot \mathbf{R})], \quad (2.24)$$

the normal-mode amplitudes are found to obey the linear set of equations

$$m\omega^2(\mathbf{q})\epsilon_\alpha(\mathbf{q}) = \sum_\beta B_{\alpha\beta}(\mathbf{q})\epsilon_\beta(\mathbf{q}). \quad (2.25)$$

For any \mathbf{q} , the three eigenvalues of $B_{\alpha\beta}(\mathbf{q})$, namely $m\omega_s^2(\mathbf{q})$ ($s = 1, 2, 3$), are real and we can always choose orthonormal eigenvectors, $\sum_\alpha \epsilon_{s\alpha}(\mathbf{q})\epsilon_{s'\alpha}(\mathbf{q}) = \delta_{ss'}$. The explicit form of the dynamical-matrix components is $B_{\alpha\alpha} = \tau_{\alpha\alpha} - \tau_1$ and $B_{\alpha\beta} = \tau_{\alpha\beta}$ ($\alpha \neq \beta$), where

$$\begin{aligned} \tau_1(\mathbf{q}) &= - \sum_{n \neq 1} \frac{\phi'(|\mathbf{R}_n|)}{|\mathbf{R}_n|} [1 - \cos(\mathbf{q} \cdot \mathbf{R}_n)] ; \\ \tau_{\alpha\beta}(\mathbf{q}) &= \sum_{n \neq 1} \frac{X_\alpha X_\beta}{|\mathbf{R}_n|^4} [|\mathbf{R}_n|^2 \phi''(|\mathbf{R}_n|) - |\mathbf{R}_n| \phi'(|\mathbf{R}_n|)] [1 - \cos(\mathbf{q} \cdot \mathbf{R}_n)]. \end{aligned} \quad (2.26)$$

A crystal dynamics is also associated with the approximation set by linear elasticity. It is drawn from the Lagrangian density (cf. Eq. (2.12))

$$\mathcal{L} = \frac{1}{2}\rho \dot{u}^2(\mathbf{x}) - \sum_{\alpha,\beta} S_{\alpha\beta} u_{\alpha\beta} - \frac{1}{2} \sum_{\alpha,\beta,\gamma,\delta} S_{\alpha\beta\gamma\delta} u_{\alpha\beta} u_{\gamma\delta}, \quad (2.27)$$

where ρ is the mass density. From Eq. (2.27) one derives the equations of motion

$$\rho \ddot{u}_\alpha(\mathbf{x}) = \sum_{\beta,\gamma,\delta} c_{\alpha\beta\gamma\delta} \frac{\partial^2 u_\gamma}{\partial x_\beta \partial x_\delta}, \quad (2.28)$$

whose solutions of are still plane waves with frequencies given by the secular equation

$$\det \left\{ \sum_{\beta\delta} c_{\alpha\beta\gamma\delta} q_\beta q_\delta - \rho \omega^2(\mathbf{q}) \delta_{\alpha\gamma} \right\} = 0. \quad (2.29)$$

In particular, one observes that the elastic waves are dispersionless, *i.e.*, $\omega^2 \propto q^2$. For cubic crystals, the explicit form of Eq. (2.29) is:

$$\begin{vmatrix} c_{11}q_x^2 + c_{44}(q_y^2 + q_z^2) - \rho\omega^2 & (c_{12} + c_{44})q_xq_y & (c_{12} + c_{44})q_xq_z \\ (c_{12} + c_{44})q_xq_y & c_{11}q_y^2 + c_{44}(q_x^2 + q_z^2) - \rho\omega^2 & (c_{12} + c_{44})q_yq_z \\ (c_{12} + c_{44})q_xq_z & (c_{12} + c_{44})q_yq_z & c_{11}q_z^2 + c_{44}(q_x^2 + q_y^2) - \rho\omega^2 \end{vmatrix} = 0. \quad (2.30)$$

III. A NEW MELTING CRITERION

In this Section, a Gaussian field theory is formulated in order to describe the thermal properties of an elastic solid in the simplest possible terms. The aim is to obtain an approximate value for the mean square displacement (MSD) of crystal atoms that can be used to estimate the melting temperature of the crystal through the Lindemann criterion.

Consider for concreteness a crystal of cubic symmetry with $N = N_1 N_2 N_3$ atoms. Rather than assuming a homogeneous strain, I allow for a spatial dependence of atomic displacements and take the continuum limit. Then, the enthalpy H of the crystal at $T = 0$ becomes (cf. Eq. (2.4)):

$$\begin{aligned}
H = H_0 + \frac{1}{2} \int_{V_0} d^3 r \left\{ \lambda_1 \left[\left(\frac{\partial u_x}{\partial x} \right)^2 + \left(\frac{\partial u_y}{\partial y} \right)^2 + \left(\frac{\partial u_z}{\partial z} \right)^2 \right] \right. \\
+ 2\lambda_2 \left(\frac{\partial u_x}{\partial x} \frac{\partial u_y}{\partial y} + \frac{\partial u_x}{\partial x} \frac{\partial u_z}{\partial z} + \frac{\partial u_y}{\partial y} \frac{\partial u_z}{\partial z} \right) \\
\left. + \lambda_3 \left[\left(\frac{\partial u_x}{\partial y} + \frac{\partial u_y}{\partial x} \right)^2 + \left(\frac{\partial u_x}{\partial z} + \frac{\partial u_z}{\partial x} \right)^2 + \left(\frac{\partial u_y}{\partial z} + \frac{\partial u_z}{\partial y} \right)^2 \right] \right\} \quad (3.1)
\end{aligned}$$

with the λ 's given by Eq. (2.6). Upon implementing periodic boundary conditions, the displacement vector is expanded in a series of plane waves:

$$u_\alpha(\mathbf{r}) = \sum_{\mathbf{q}} \tilde{u}_\alpha(\mathbf{q}) e^{i\mathbf{q}\cdot\mathbf{r}} \quad (\text{conversely, } \tilde{u}_\alpha(\mathbf{q}) = \frac{1}{V_0} \int_{V_0} d^3 r u_\alpha(\mathbf{r}) e^{-i\mathbf{q}\cdot\mathbf{r}}), \quad (3.2)$$

where, in terms of reciprocal-lattice primitive vectors, the wave vector $\mathbf{q} = \sum_\alpha q_\alpha \mathbf{b}_\alpha$ with $q_\alpha = m_\alpha / N_\alpha$ and $m_\alpha = -N_\alpha/2 + 1, \dots, N_\alpha/2$ ($\alpha = 1, 2, 3$). Substitution of (3.2) into (3.1) leads eventually to

$$H = H_0 + \frac{1}{2} V_0 \sum_{\mathbf{q}} \sum_{\alpha, \beta} A_{\alpha\beta}(\mathbf{q}) \tilde{u}_\alpha(\mathbf{q}) \tilde{u}_\beta^*(\mathbf{q}) \quad (3.3)$$

with

$$A_{\alpha\beta}(\mathbf{q}) = [\lambda_3 q^2 + (\lambda_1 - \lambda_2 - 2\lambda_3) q_\alpha^2] \delta_{\alpha\beta} + (\lambda_2 + \lambda_3) q_\alpha q_\beta. \quad (3.4)$$

Next, I try to represent the thermal disordering of the crystal through a field theory where the basic variables are the $u_\alpha(\mathbf{r})$'s and the statistical weight of field configurations is $\exp(-\beta H)$. This choice is tantamount to the assumption of T -independent elastic constants, whose values are fixed at their (P -dependent) $T = 0$ values.

To compute the MSD, the following average is to be evaluated first:

$$\langle \tilde{u}_\alpha(\mathbf{q}) \tilde{u}_\beta^*(\mathbf{q}) \rangle = \frac{\int \mathcal{D}\tilde{u} \mathcal{D}\tilde{u}^* \tilde{u}_\alpha(\mathbf{q}) \tilde{u}_\beta^*(\mathbf{q}) \exp\{-\beta V_0 \sum_{\mathbf{q}>0} \sum_{\gamma, \delta} A_{\gamma\delta}(\mathbf{q}) \tilde{u}_\gamma(\mathbf{q}) \tilde{u}_\delta^*(\mathbf{q})\}}{\int \mathcal{D}\tilde{u} \mathcal{D}\tilde{u}^* \exp\{-\beta V_0 \sum_{\mathbf{q}>0} \sum_{\gamma, \delta} A_{\gamma\delta}(\mathbf{q}) \tilde{u}_\gamma(\mathbf{q}) \tilde{u}_\delta^*(\mathbf{q})\}}, \quad (3.5)$$

where in both integrals the \mathbf{q} 's are restricted to half space (symbolically, $\mathbf{q} > 0$) in order that $\{\text{Re } \tilde{u}_\alpha(\mathbf{q}), \text{Im } \tilde{u}_\alpha(\mathbf{q})\}$ can be treated as independent integration variables – namely, $\mathcal{D}\tilde{u} \mathcal{D}\tilde{u}^* = \prod_{\mathbf{q}>0} \prod_\alpha d(\text{Re } \tilde{u}_\alpha(\mathbf{q})) d(\text{Im } \tilde{u}_\alpha(\mathbf{q}))$. Using properties of complex-valued Gaussian integrals, one obtains

$$\langle \tilde{u}_\alpha(\mathbf{q}) \tilde{u}_\beta^*(\mathbf{q}) \rangle = \frac{k_B T}{V_0} (A^{-1})_{\alpha\beta}(\mathbf{q}). \quad (3.6)$$

Since the inverse of a symmetric matrix is also symmetric, the previous result actually applies for any \mathbf{q} . Hence, the MSD reads

$$\left\langle \frac{1}{V_0} \int_{V_0} d^3r u^2(\mathbf{r}) \right\rangle = \sum_{\mathbf{q}} \sum_{\alpha} \langle |\tilde{u}_{\alpha}(\mathbf{q})|^2 \rangle = \frac{k_B T}{V_0} \sum_{\mathbf{q}} \text{Tr} A^{-1}(\mathbf{q}). \quad (3.7)$$

In the thermodynamic limit, the residual sum transforms into an integral over the 1BZ, which is more easily computed by replacing the zone with a (Debye) sphere of equal volume (the error committed is small), with the result:

$$\left\langle \frac{1}{V_0} \int_{V_0} d^3r u^2(\mathbf{r}) \right\rangle = \frac{k_B T}{\pi^3} q_D \int_0^{\pi/2} d\phi \int_0^{\pi/2} d\theta \sin \theta \frac{f_1(\theta, \phi)}{f_2(\theta, \phi)}, \quad (3.8)$$

where $q_D = (6\pi^2\rho)^{1/3}$ and

$$\begin{aligned} f_1(\theta, \phi) &= \lambda_3(\lambda_3 + 2\lambda_1) + (\lambda_1 + \lambda_2)(\lambda_1 - \lambda_2 - 2\lambda_3)(\sin^4 \theta \sin^2 \phi \cos^2 \phi + \sin^2 \theta \cos^2 \theta); \\ f_2(\theta, \phi) &= \lambda_1 \lambda_3^2 + \lambda_3(\lambda_1 + \lambda_2)(\lambda_1 - \lambda_2 - 2\lambda_3)(\sin^4 \theta \sin^2 \phi \cos^2 \phi + \sin^2 \theta \cos^2 \theta) \\ &\quad + (\lambda_1 - \lambda_2 - 2\lambda_3)^2(\lambda_1 + 2\lambda_2 + \lambda_3) \sin^4 \theta \cos^2 \theta \sin^2 \phi \cos^2 \phi. \end{aligned} \quad (3.9)$$

The parallel treatment for a harmonic crystal moves from

$$U = U_0 + \frac{N}{2} \sum_{\mathbf{q}} \sum_{\alpha, \beta} B_{\alpha\beta}(\mathbf{q}) \tilde{u}_{\alpha}(\mathbf{q}) \tilde{u}_{\beta}^*(\mathbf{q}), \quad (3.10)$$

and eventually leads, through the same series of steps as before, to the following expression for the MSD,

$$\left\langle \frac{1}{N} \sum_{\mathbf{R}} u^2(\mathbf{R}) \right\rangle = \frac{k_B T}{(2\pi)^3} v_0 \int_0^{q_D} dq q^2 \int d^2\Omega \text{Tr} B^{-1}(\mathbf{q}), \quad (3.11)$$

which is more numerically demanding than (3.8) because of the additional q integration present in (3.11).

We see from Eqs. (3.8) and (3.11) that the MSD increases linearly with T . According to the Lindemann criterion, the crystal melts when the MSD reaches a fraction $L_m \approx 0.1$ of the nearest-neighbour distance a_{NN} , from which the estimate of $T_m(P)$ follows directly. For face-centred cubic (fcc), hexagonal close-packed (hcp), and body-centred cubic (bcc) crystals, the specific L_m values are 0.15, 0.10, and 0.18, respectively [10, 11], while no systematic study of the typical values of the Lindemann ratio for other crystals has ever been undertaken, at least to my knowledge (hence, I assume $L_m = 0.1$ indifferently for all such phases). If any of

the stability conditions is violated for a crystal under pressure P_0 , then I take a zero melting temperature for the given solid at $P = P_0$.

Universality of L_m along the fluid-solid coexistence line is well established for fcc, bcc, and hcp crystals. For other types of crystals no such information is available and this makes the T_m estimated through what I shall call *the elastic criterion of melting* less reliable for these crystals. In general, the elastic constants get smaller and smaller on increasing temperature until they abruptly vanish on crossing the melting line. Hence, assuming the elastic constants to be independent of T is a major simplification that leads to systematically underestimating the MSD; moreover, also the neglect of anharmonic terms in the potential would likely contribute to enhancing the stability of the solid, with the effect that the $T_m(P)$ computed with the elastic criterion of melting will be larger than the actual value. One may reasonably expect that the extent to which the melting temperature is overestimated is roughly the same for all pressures so that at least the shape of $T_m(P)$ is got correctly.

A first application of the elastic criterion is to the melting of the Lennard-Jones fluid, which is known to crystallize into a hcp solid (unless the pressure is huge – larger than 800 in reduced ϵ/σ^3 units). For reduced pressures smaller than 20, the computed T_m is a concave function of P , as expected [12]. For $P = 1$ and $P = 10$, the criterion predicts a melting temperature of 1.18 and 1.75, respectively, whereas the “exact” values from Ref. [12] are 0.78 and 1.40.

A more challenging test of the elastic criterion is offered by a recent simulation study [7] of a system of particles repelling each other through the Yoshida-Kamakura (YK) potential,

$$\phi_{\text{YK}}(r) = \epsilon \exp \left[a \left(1 - \frac{r}{\sigma} \right) - 6 \left(1 - \frac{r}{\sigma} \right)^2 \ln \frac{r}{\sigma} \right] \quad (3.12)$$

with $a = 3.3$. For reduced pressures smaller than 3, the phase diagram of the model is plotted in figure 3 of Ref. [7]. The same phase diagram but computed through the present melting criterion (with an enormous saving of time compared to simulation) is reported in Fig. 1. Here are shown the melting lines for a number of solid phases chosen among those stable at zero temperature. For each crystal, the melting curve is a single line or it consists of a number of disjoint pieces, one for each range of pressure/density where the stability conditions are met. It is worth stressing that the pressure range of mechanical stability of a phase is usually wider than the range of *thermodynamic* stability at $T = 0$, which is where the enthalpy of the phase is smaller than that of any other crystal phase. Hence,

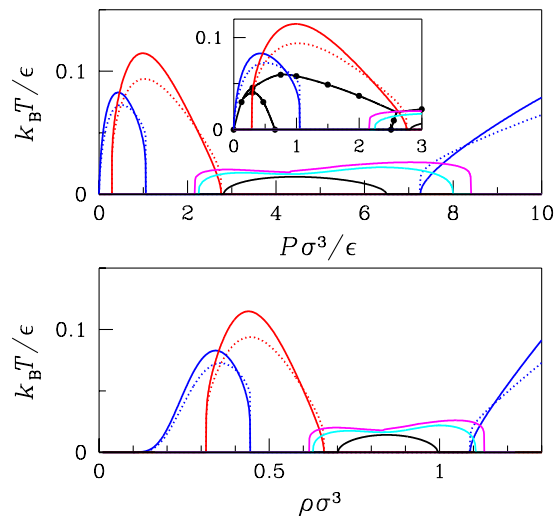


FIG. 1: (Color online). Schematic phase diagram of the YK potential with $a = 3.3$ as drawn from the elastic criterion of melting. The melting lines of various solid phases are shown: fcc (blue), bcc (red), simple cubic (sc, black), sh (cyan), and β -Sn (magenta). The dotted lines are the melting curves for the fcc and bcc crystals as derived from the harmonic approximation, see Eq. (3.11). In the inset (top panel), a comparison is made with the exact coexistence boundaries of the model (black dots and thick solid lines) [7]. From low to high pressure, the stable phases up to $P = 3$ are fcc, bcc, and β -Sn.

the stability boundaries dictated by the elastic criterion do not generally coincide with the actual thermodynamic thresholds.

On approaching a stability boundary, the MSD of Eq. (3.8) blows up and the melting temperature drops continuously to zero. The line of fluid-solid coexistence would correspond to the upper envelope of the melting curves for the various solids. It is clear from Fig. 1 that the gross features of the phase diagram of the YK fluid are well reproduced by the elastic criterion, the main error being in the regular overestimation of the melting temperature. The greater stability of the β -Sn phase over the simple hexagonal (sh) solid in the pressure range between roughly 3 and 7 might be just accidental, related to the choice of the same L_m for both. The harmonic approximation works quantitatively better (since at variance with linear elasticity no large-wavelength limit is implied) but it takes a much longer computer time to calculate the MSD.

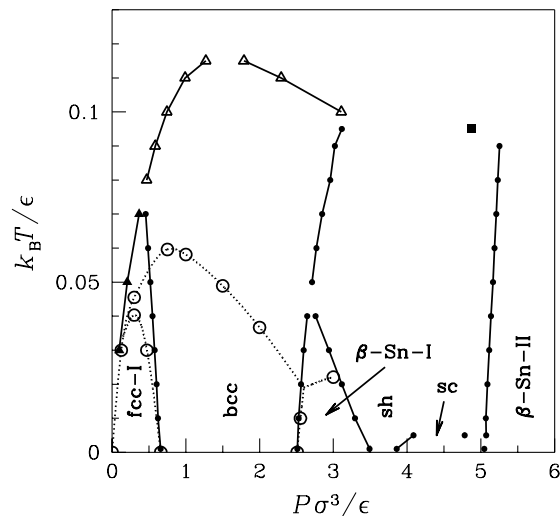


FIG. 2: Low-pressure phase diagram of the YK potential with $a = 3.3$ according to the theory detailed in the Appendix. Solid-solid coexistence points are depicted as small dots, whereas triangles and the full square are solid-fluid coexistence points. When there are more than one crystal phase of a given type, a Roman numeral distinguishes between them (e.g. β -Sn-I and β -Sn-II; the second fcc phase is stable for pressures out of the range shown). The dotted lines through the open dots are the coexistence loci of the model from Ref. [7].

To better appreciate the quality of the elastic criterion of melting, it is worth considering what would be the phase diagram of the YK potential with $a = 3.3$ according to a theory of fluid-solid coexistence based on the use of the cell-theory approximation for the solid and the Mansoori-Canfield theory for the fluid (see the details in the Appendix). We see from Fig. 2 that this theory predicts a direct transition from bcc to sh at high temperature, a possibility which was not actually considered in the simulation; however, the melting temperature of the YK fluid is overestimated by the theory to roughly the same extent ($\approx 100\%$) as it is by the elastic criterion, a fact that alone casts some shadows on the reliability of the theoretical phase diagram.

It is instructive to look at the shape of some representative phonon branches of the bcc crystal of YK particles for $\rho = 0.6607$ ($P \simeq 2.76$), *i.e.*, where the bcc solid is about to become unstable at zero temperature owing to the fact that c_{44} is almost zero and actually negative for larger pressures. This instability is caused by phonon softening at the Γ point:

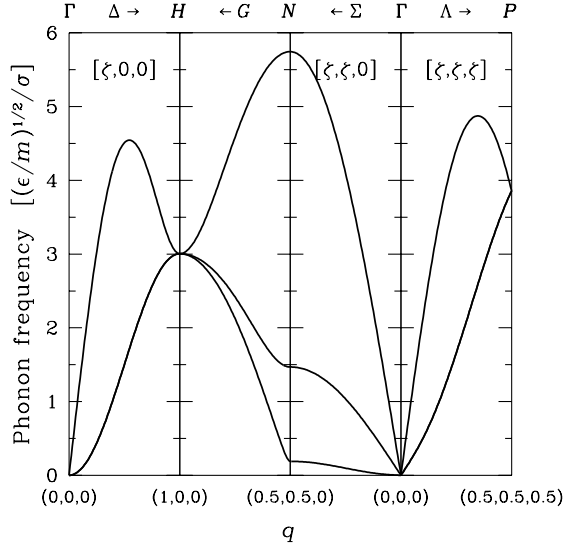


FIG. 3: Yoshida-Kamakura potential (3.12) with $a = 3.3$: phonon branches of the BCC crystal for $\rho = 0.6607$ along a number of high-symmetry lines in \mathbf{q} space. Along the ΓN path, one of the branches is seen to soften at the Γ point due to the vanishing of c_{44} .

along the path from Γ to N , one of the phonon branches satisfies $m\omega^2(\mathbf{q}) \simeq (c_{44}/\rho)(q_x^2 + q_y^2)$ for $q \rightarrow 0$ (see Fig. 3).

Upon varying the value of a in Eq. (3.12), one can follow the evolution of the YK phase diagram through the elastic criterion of melting [7]. For large a values, the inverse-power-fluid limit is recovered; for $a \simeq 7$, there appears a region of bcc stability between the low- and high-density fcc solids; on decreasing a more and more, the stable-bcc region gradually shrinks until, for $a \approx 4$, a gap opens between the bcc and high-density fcc regions, signalling the stabilization for intermediate pressures of one or more crystals of symmetry other than cubic. The opening of the gap is preceded by the onset of reentrant melting, which first occurs for $a \approx 5$.

Another instance of core-softened repulsion is provided by the modified inverse-power (MIP) potential studied in Ref. [13]. The following one-parameter family of potentials is being considered:

$$\phi_{\text{MIP}}(r) = \epsilon \left(\frac{\sigma}{r}\right)^{n(r)} \quad \text{with } n(r) = 12 \left\{ 1 - a \exp \left[-5 \left(1 - \frac{r}{\sigma}\right)^2 \right] \right\}, \quad (3.13)$$

where $0 < a < 1$ is a softness parameter, *i.e.*, a number fixing the extent to which the inverse-power exponent deviates from 12 in the close neighbourhood of σ . Upon increasing

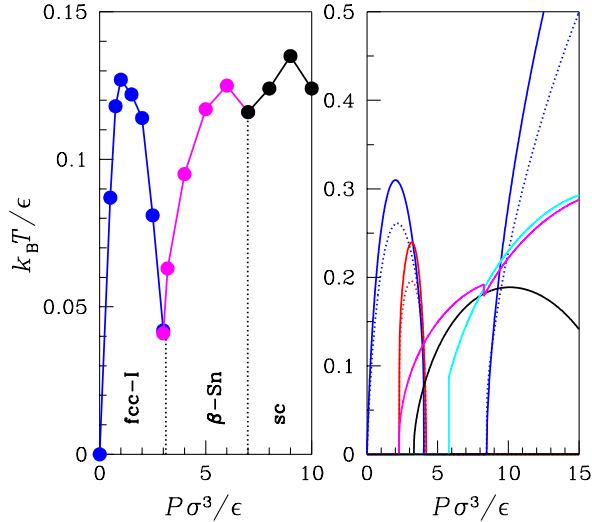


FIG. 4: (Color online). Modified inverse-power potential with $a = 0.8$. Left: Numerically-computed phase diagram (reprinted from Ref. [13]; the dots are melting points as obtained by the heat-until-it-melts method while the vertical dotted lines are putative solid-solid boundaries as extrapolated from exact total-energy calculations at $T = 0$); right: same phase diagram as predicted through the elastic criterion of melting (blue, fcc; red, bcc; black, sc; cyan, sh; magenta, β -Sn; the blue and red dotted lines are the melting curves for the fcc and bcc crystals, respectively, as drawn from the harmonic approximation).

a , the potential core softens more and more, with the effect of destabilizing both the fcc and the bcc order for intermediate densities. This is accompanied by reentrant melting and by the appearance of one or more low-coordinated crystal phases in the pressure gap left open by bcc and fcc. In the left panel of Fig. 4, I report the phase diagram of the MIP fluid for $a = 0.8$ as obtained from Monte Carlo simulation through the heat-until-it-melts method [13]; the same melting lines but derived from the elastic criterion are plotted in the right panel of Fig. 4. Again, we see more than one correspondence between the present melting criterion and the simulation results.

However, there are also instances (arguably not so common) where the elastic criterion fails badly. This occurs when a crystal that is predicted by linear elasticity to be unstable at $T = 0$ is in fact stabilized in a range of temperatures, somewhat counterintuitively, by virtue of anharmonic effects. In a case of these, anharmonicity manages to make a crystal

TABLE I: MIP potential for $a = 0.6$, elastic constants of the BCC crystal at the reduced densities $\rho = 0.7$ and $\rho = 1$. The exact $T = 0$ values derived from Eqs. (2.6) are compared with their MC estimates at $T = 0.001$ (for samples of $N = 686$ particles and equilibrium trajectories of as many as 2×10^5 MC moves per particle). While the BCC crystal would be mechanically unstable at $\rho = 1$ according to elasticity theory, it is actually found perfectly rigid to thermal fluctuations in numerical simulation owing to the stabilizing effect of the anharmonicities in the potential.

	$\rho = 0.7$			$\rho = 1$		
	c_{11}	c_{12}	c_{44}	c_{11}	c_{12}	c_{44}
$T = 0$	10.06156	8.64219	2.94964	18.92754	13.80805	-0.41631
MC	10.046(1)	8.632(1)	2.937(1)	18.1(3)	13.89(3)	0.955(4)

phase rigid to small deformations in spite of the violation of the stability conditions of elasticity. I found one case of these for the MIP potential. The $T = 0$ calculation of the bcc elastic moduli for $a = 0.6$ predicts a gap of stability in the density range from $\rho = 0.910$ ($P \simeq 5.761$) to $\rho = 1.066$ ($P \simeq 8.168$), whereas for e.g. $\rho = 1$ ($P \simeq 7.021$ at $T = 0$) Monte Carlo simulation clearly indicates that the bcc solid is stable up to $T \simeq 0.105$ [13] (all quantities in reduced units). A numerical calculation of the elastic constants for $\rho = 1$ at very low temperature ($T = 0.001$) with the method of Ref. [9] indeed reveals large deviations from the $T = 0$ values, which is not the case for e.g. $\rho = 0.7$ ($P \simeq 2.846$ at $T = 0$), where the agreement with linear elasticity is much better (see Table 1). What is happening then? The similar situation with Calcium sc phase provides a clue [14]: strong enough anharmonic terms in the Hamiltonian (classical or quantum) may succeed to convert imaginary phonon frequencies into real ones, thus allowing the alleged unstable solid to become mechanically (and thermodynamically) stable.

IV. THE MELTING CURVE OF THE GAUSSIAN-CORE MODEL

The Gaussian-core model (GCM) fluid (*i.e.*, classical point particles interacting through a repulsive Gaussian potential in three dimensions) gives the opportunity to compare the relative efficacy of various empirical melting rules, all rooted in the use of the Lindemann

criterion. In particular, we shall figure out the merits and drawbacks of the self-consistent harmonic approximation (SCHA) [15], which for many years represented a popular theoretical alternative to exact free-energy calculations.

Besides a fluid phase, the GCM shows two distinct, fcc and bcc solid phases [16]. At $T = 0$, the fcc solid transforms to bcc for $P = 0.05529$. At higher pressures and for $T > 0$, the bcc solid undergoes reentrant melting: $T_m(P)$ is an increasing function for $P \lesssim 0.136$ while being decreasing otherwise, further vanishing in the limit of infinite pressure. The fcc and bcc melting lines as predicted by the elastic criterion are reported in Fig. 5, together with those obtained from the harmonic approximation. In the same picture, the outcome of a variational treatment [17] and the numerically-computed coexistence lines [18] are also plotted for comparison. Clearly, the simple elastic criterion is able to account for the main characteristics of GCM melting, though the fcc and bcc melting temperatures are again found to be about twice larger than the actual values and the threshold where the fcc solid is overcome in stability by the bcc phase remains vague, much overestimated by the putative fcc reentrant-melting line. Quantitatively speaking, the harmonic approximation and, especially, the variational theory provide more valid alternatives to free-energy calculations.

The SCHA is a theory for the thermal attenuation of phonon energies that aims at introducing elements of anharmonicity in an otherwise harmonic set-up. It provides an internal, self-consistent condition for its own validity which had sometimes been interpreted as an indication of the maximum temperature at which the crystal can be superheated. When used in combination with the Lindemann rule, the SCHA provides an independent melting criterion. Before illustrating the specific prediction for the GCM, I present a brief introduction to the SCHA.

The formal justification of the SCHA lies in the use of the variational method of statistical mechanics. The strategy is focussed on determining the “optimal” harmonic approximation to the real Hamiltonian at the given temperature T , which is generally not its harmonic part. The crucial assumption is that of an integrable pair potential $\phi(\mathbf{r})$, endowed with a Fourier transform $\tilde{\phi}(\mathbf{q})$. This automatically excludes hard-core potentials, for which the SCHA theory cannot be formulated. The average of the system potential energy over a reference harmonic system U_{harm} , having the same potential-energy minimum as the system

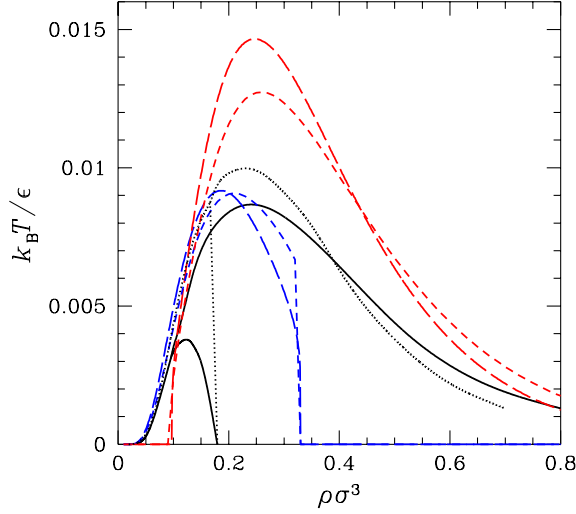


FIG. 5: (Color online). The Gaussian-core model phase diagram as determined through various methods: exact free-energy calculations (solid black lines); variational method (dotted black lines); elastic criterion of melting (long-dashed blue and red lines – blue, fcc; red, bcc); harmonic approximation (dashed blue and red lines).

of interest but *different* phonon frequencies $\omega_s(\mathbf{k})$ and normal-mode amplitudes $\epsilon_s(\mathbf{k})$, is

$$\langle U \rangle_{\text{harm}} = \frac{v_0}{2} \sum'_{i,j} \int \frac{d^3q}{(2\pi)^3} \tilde{\phi}(\mathbf{q}) e^{i\mathbf{q} \cdot (\mathbf{R}_i - \mathbf{R}_j)} e^{-\frac{1}{2} \langle (\mathbf{q} \cdot (\mathbf{u}_i - \mathbf{u}_j))^2 \rangle_{\text{harm}}}, \quad (4.1)$$

where the prime over the sum means $i \neq j$ and

$$\frac{1}{2} \langle (\mathbf{q} \cdot (\mathbf{u}_i - \mathbf{u}_j))^2 \rangle_{\text{harm}} = \frac{k_B T}{N} \sum_{\mathbf{k}, s} (\mathbf{q} \cdot \epsilon_s(\mathbf{k}))^2 \frac{1 - e^{i\mathbf{k} \cdot (\mathbf{R}_i - \mathbf{R}_j)}}{m\omega_s^2(\mathbf{k})} \equiv D(\mathbf{q}, \{\mathbf{R}\}). \quad (4.2)$$

The best approximation to the Helmholtz free energy of the system within all conceivable harmonic interactions is given by the minimum of the Gibbs-Bogoliubov functional,

$$\tilde{F}[H_{\text{harm}}] \equiv F_{\text{harm}} + \langle H - H_{\text{harm}} \rangle_{\text{harm}} = F_{\text{harm}} + \langle U \rangle_{\text{harm}} - U_0 - \frac{3}{2} N k_B T, \quad (4.3)$$

where the Helmholtz free energy of the reference system reads

$$F_{\text{harm}} = U_0 + 3N k_B T \ln \left(\frac{\Lambda}{v_0^{1/3}} \right) + \frac{k_B T}{2} \sum_{\mathbf{k}, s} \ln \left(\frac{m\omega_s^2(\mathbf{k})v_0}{\pi k_B T} \right) \quad (4.4)$$

with Λ the thermal wavelength. Using the frequencies $\omega_s(\mathbf{k})$ as variational parameters, they are eventually obtained as the solutions of the SCHA equations

$$m\omega_s^2(\mathbf{k}) = v_0 \sum_{j \neq 1} (e^{-i\mathbf{k} \cdot \mathbf{R}_j} - 1) \int \frac{d^3q}{(2\pi)^3} (\mathbf{q} \cdot \boldsymbol{\epsilon}_s(\mathbf{k}))^2 \tilde{\phi}(\mathbf{q}) e^{-i\mathbf{q} \cdot \mathbf{R}_j} e^{-D(\mathbf{q}, \{\mathbf{R}\})}. \quad (4.5)$$

In practice, the target temperature T is reached in steps, where at every step of the calculation the equations (4.5) are solved iteratively until the left-hand side equates to a certain degree of precision the right-hand side. At low temperature, a good starting point of the iteration are the system own frequencies. Observe that, thanks to symmetry considerations, a (congruous) number of \mathbf{k} vectors in a small fraction of the 1BZ will suffice for the calculation of a sum like that in D (e.g. just 1/48 of the full 1BZ for the FCC lattice) [19]. Once D is obtained, the matrix

$$Z_{\alpha\beta}(\mathbf{k}) = v_0 \sum_{j \neq 1} (\cos(\mathbf{k} \cdot \mathbf{R}_j) - 1) \int \frac{d^3q}{(2\pi)^3} q_\alpha q_\beta \tilde{\phi}(\mathbf{q}) \cos(\mathbf{q} \cdot \mathbf{R}_j) e^{-D} \quad (4.6)$$

is diagonalized in order to extract its eigenvalues $m\omega_s^2(\mathbf{k})$ and eigenvectors $\boldsymbol{\epsilon}_s(\mathbf{k})$, and this completes a single iteration step.

The main limitation in the use of the SCHA method is computational, due to the necessity of solving numerically a large number of times the integral in (4.6) to a high degree of precision. In the GCM case this integral can be computed analytically and this enormously speeds up the whole procedure. Even in this favourable situation, computing a single melting point by the SCHA method takes a time typically three orders of magnitude larger than if we apply the elastic criterion, which performs the calculation in a few hundredths of a second on a fast PC. In general, for a given density ρ the self-consistent calculation of the frequencies $\omega_s(\mathbf{k})$ and the respective MSD can be accomplished only up to a certain temperature $T_i(\rho)$, which is called the instability temperature. Beyond this temperature, no self-consistent solution of the Eqs. (4.5) is found. Moreover, depending on ρ the ratio of the MSD at T_i to a_{NN} may even exceed L_m (in this event, I assume $T_m = T_i$). The SCHA results for the GCM are reported in Fig. 6. Compared to the outcome of the elastic criterion, the SCHA estimate of the GCM melting temperature is better for all low to intermediate densities; the SCHA is instead unable to reproduce the large-density tail of $T_m(P)$ since beyond a density of 0.57 I find no self-consistent solution of the Eqs. (4.5) and the relative T_m hence drops to zero. It is worth adding a final remark about the SCHA instability thresholds for the GCM model. As we see from Fig. 6, the T_i for fcc is higher than it is for bcc, in sharp contrast with

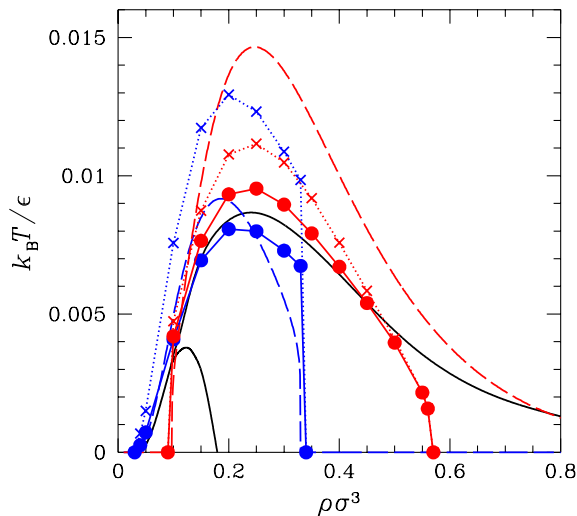


FIG. 6: (Color online). Gaussian-core model phase diagram: the outcome of the SCHA (blue and red dots, joined by solid straight lines – blue, fcc; red, bcc) is compared with that of the elastic criterion of melting (long-dashed blue and red lines). The SCHA instability temperatures for the fcc and bcc solids are also plotted as blue and red crosses, respectively, joined by dotted straight lines. Finally, the solid black lines mark the exact coexistence loci.

the sequence of melting thresholds. In fact, the SCHA instability at, say, $\rho\sigma^3 = 0.2$ occurs, for both phases, where the root mean square displacement (rmsd) for the reference system is roughly a fraction 0.23 of the nominal NN distance (r_{NN}). But the rate of growth with temperature of rmsd/r_{NN} is slightly larger for bcc, with a pronounced acceleration above a level of about 0.17 for bcc and 0.20 for fcc; hence, the rmsd/r_{NN} of the bcc crystal reaches the values 0.18 (melting) and 0.23 (instability) both within the range comprised between the fcc melting and instability temperatures.

V. CONCLUSIONS

Through the use of representative model potentials, I managed to show that a simple melting criterion based on the Lindemann rule and a description of the solid as an elastic medium is able to capture, with negligible computational effort, the overall characteristics of the system melting line. In more quantitative terms, the criterion overestimates the

melting temperature by roughly a factor of two for fcc and bcc solids, independently of the pressure value. For other crystals, the prediction of the criterion is less reliable, mainly due to the uncertainty on the value of the Lindemann parameter and its actual pressure dependence. In fact, the value of the elastic criterion of melting is more of a heuristic kind, *i.e.*, of guidance for fastly detecting the existence of anomalies in the melting line, as in case of reentrant-fluid behaviour in a system where the softness of the particle core can be made to vary by tuning an appropriate parameter in the potential. The accuracy obtained by the elastic criterion in predicting the overall appearance of the phase diagram can be comparable to that of more sophisticated (two-phase) theories of fluid-solid coexistence, as I showed for one instance of core-softened interaction. For a Gaussian repulsive core, I compared the outcome of the elastic criterion with the harmonic approximation, as well as with the more effective but also more numerically demanding self-consistent harmonic approximation. Though moving upward in the hierarchy of theories generally improves the estimate of the melting temperature for all pressures, the gain in accuracy is only marginal and, more important, the topology of the melting line stays unaltered. Hence, at least for the Gaussian potential, a description in terms of zero-temperature elastic constants is by far sufficient to anticipate the essential features of the melting behaviour and no better theory is strictly necessary.

Appendix A: A statistical theory of the fluid-solid transition

In this Appendix, a theory of fluid-solid coexistence is formulated for purely repulsive potentials, where the fluid phase is described through the variational approach by Mansoori and Canfield [20] while the statistical properties of each solid phase are modelled through a cell theory.

Assuming the hard-sphere (HS) fluid as reference, it derives from the Gibbs-Bogoliubov inequality that the exact Helmholtz free energy per particle f of a system with potential $\phi(r)$ is bounded from above by

$$f^*(T, v; \sigma_{\text{HS}}) = f_{\text{HS}} + \frac{\rho}{2} \int d^3r g_{\text{HS}}(r) w(r) \quad \text{with } w(r) = \phi(r) - \phi_{\text{HS}}(r), \quad (\text{A.1})$$

where $\rho = 1/v$ is the number density and $g_{\text{HS}}(r)$ is the HS radial distribution function (RDF). In Eq. (A.1), the HS particle diameter σ_{HS} is left unspecified; the best approximant

to f is obtained by minimizing (A.1) with respect to σ_{HS} . Although the HS equation of state is not known exactly, a good approximation is the Carnahan-Starling form [3] from which the HS free energy follows as

$$f_{\text{HS}} = k_B T [\ln(\rho \Lambda^3) - 1] + k_B T \frac{\eta(4 - 3\eta)}{(1 - \eta)^2} \quad (\text{A.2})$$

with $\eta = (\pi/6)\rho\sigma_{\text{HS}}^3$. To obtain an estimate of the HS RDF, one resorts to the Percus-Yevick approximation [3] since then the direct correlation function $c_{\text{HS}}(r) = c_0(r/\sigma_{\text{HS}}; \eta)$ is known in a closed form:

$$c_0(x) = \begin{cases} -\lambda_0 - \lambda_1 x - \lambda_3 x^3, & x < 1 \\ 0, & x \geq 1 \end{cases} \quad (\text{A.3})$$

with $\lambda_0 = \frac{(1 + 2\eta)^2}{(1 - \eta)^4}$, $\lambda_1 = -6\eta \frac{(1 + \eta/2)^2}{(1 - \eta)^4}$, $\lambda_3 = \eta \frac{\lambda_0}{2}$.

The Ornstein-Zernike relation then yields $g_{\text{HS}}(r) = g_0(r/\sigma_{\text{HS}}; \eta)$ with

$$g_0(x) = 1 + \frac{2}{\pi} \int_0^\infty dk k^2 \frac{\sin(kx)}{kx} \frac{\tilde{c}_0(k)}{1 - 24\eta\tilde{c}_0(k)} \quad \text{and} \quad \tilde{c}_0(k) = \int_0^1 dx x^2 \frac{\sin(kx)}{kx} c_0(x). \quad (\text{A.4})$$

The variational free energy (A.1) can then be written as

$$\begin{aligned} f^* &= k_B T [\ln(\rho \Lambda^3) - 1] + k_B T \frac{\eta(4 - 3\eta)}{(1 - \eta)^2} + 12\eta \int_1^\infty dx x^2 g_0(x; \eta) \phi(x\sigma_{\text{HS}}) \\ &\equiv 3k_B T \ln \frac{\Lambda}{\sigma} + k_B T [\ln(\rho \sigma^3) - 1] + \Delta f^*, \end{aligned} \quad (\text{A.5})$$

where σ is an arbitrary length unit. Called $\bar{\sigma}_{\text{HS}}(T, v)$ the optimal σ_{HS} value and observing that Δf^* depends on v only through η (*i.e.*, $\Delta f^*(T, v; \sigma_{\text{HS}}) = \varphi(T, \eta(v, \sigma_{\text{HS}}); \sigma_{\text{HS}})$), the fluid chemical potential can be approximated as $\mu = \bar{f} + \bar{P}v$, where $\bar{f} = f^*(T, v; \bar{\sigma}_{\text{HS}}(T, v))$ and $\bar{P} = -\partial \bar{f} / \partial v$. In order to calculate \bar{P} , one considers that

$$\left. \frac{\partial \Delta f^*}{\partial \sigma_{\text{HS}}} \right|_{T, v} = 0 \quad \text{whence} \quad \left. \frac{\partial \varphi}{\partial \eta} \right|_{T, \sigma_{\text{HS}}} = -\frac{\sigma_{\text{HS}}}{3\eta} \left. \frac{\partial \varphi}{\partial \sigma_{\text{HS}}} \right|_{T, \eta}. \quad (\text{A.6})$$

As a result,

$$\begin{aligned} \bar{P}v &\equiv -v \left. \frac{\partial \bar{f}}{\partial v} \right|_T = k_B T - v \left. \frac{\partial \Delta \bar{f}}{\partial v} \right|_T = k_B T - \frac{\sigma_{\text{HS}}}{3} \left. \frac{\partial \varphi}{\partial \sigma_{\text{HS}}} \right|_{T, \eta} \\ &= k_B T - \frac{2\pi}{3} \frac{\sigma_{\text{HS}}^4}{v} \int_1^\infty dx x^3 g_0(x; \eta) \phi'(x\sigma_{\text{HS}}). \end{aligned} \quad (\text{A.7})$$

This completes the derivation of an approximate expression of the fluid chemical potential to be compared with the chemical potential of the solid phase.

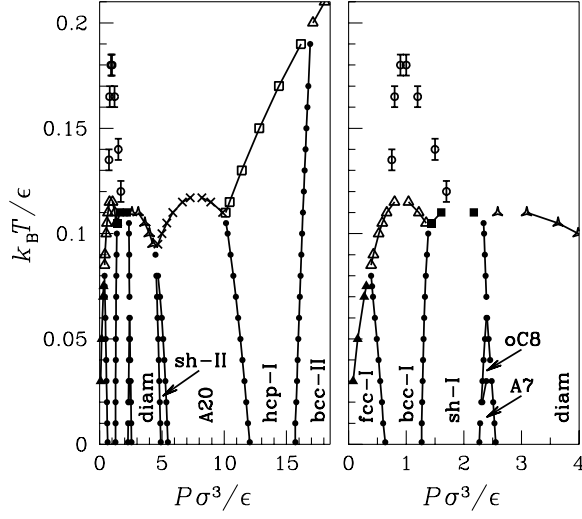


FIG. 7: Left: phase diagram of the YK potential with $a = 2.1$ according to the theory detailed in the Appendix (for the meaning of Roman numerals, see Fig.2 caption). Right: zoom on the low-pressure region. Solid-solid coexistence points are depicted as small dots, whereas triangles, squares, tripods, and crosses are solid-fluid coexistence points. See Ref. [23] for a comparison with the prediction from Monte Carlo simulation. The open dots with error bars give the location of number-density maxima within the Mansoori-Canfield description of the fluid phase.

As far as the solid sector of the phase diagram is considered, I first determine the stable phases at $T = 0$ through a series of total-energy calculations for a large number of candidate crystal structures (see Ref. [21] for more details). To obtain a rough estimate of the crystal chemical potential at $T > 0$, I use the simple Lennard-Jones-Devonshire cell theory [22]. In this theory, a crystal partition function of effectively independent particles is written down where any given particle, which can be found anywhere in its own Wigner-Seitz cell (WSC), is acted upon by the force exerted by the other $N - 1$ particles, placed at equilibrium lattice positions. In practice, the canonical partition function of a crystal is approximated as

$$Z = \frac{1}{\Lambda^{3N}} \int_{\text{WSC}_1} d^3 r_1 \cdots \int_{\text{WSC}_N} d^3 r_N \exp \left\{ - \sum_i \tilde{\phi}(\mathbf{r}_i) / (k_B T) \right\}, \quad (\text{A.8})$$

where

$$\tilde{\phi}(\mathbf{r}) = \frac{1}{2} \sum_{j \neq 1} \phi(|\mathbf{R}_1 - \mathbf{R}_j|) + \sum_{j \neq 1} [\phi(|\mathbf{R}_1 + \mathbf{r} - \mathbf{R}_j|) - \phi(|\mathbf{R}_1 - \mathbf{R}_j|)]. \quad (\text{A.9})$$

Taking

$$\Phi(\mathbf{r}) = \sum_{j \neq 1} \phi(|\mathbf{R}_1 + \mathbf{r} - \mathbf{R}_j|) \quad \text{and} \quad \Psi(\mathbf{r}) = -\frac{1}{3} \sum_{j \neq 1} |\mathbf{R}_1 + \mathbf{r} - \mathbf{R}_j| \phi'(|\mathbf{R}_1 + \mathbf{r} - \mathbf{R}_j|), \quad (\text{A.10})$$

a direct calculation offers

$$\frac{F}{N} = -k_B T \ln \frac{v_f}{\Lambda^3} + \frac{1}{2} \Phi(0) \quad \text{with} \quad v_f = \int_{\text{WSC}} d^3 r \exp\{-\beta[\Phi(\mathbf{r}) - \Phi(0)]\} \quad (\text{A.11})$$

and

$$\begin{aligned} \mu = \frac{F}{N} + Pv = & 3k_B T \ln \frac{\Lambda}{\sigma} - k_B T \left(\ln \frac{v_f}{\sigma^3} - 1 \right) + \frac{1}{2} [\Phi(0) + \Psi(0)] \\ & + \frac{\int_{\text{WSC}} d^3 r [\Psi(\mathbf{r}) - \Psi(0)] \exp\{-\beta[\Phi(\mathbf{r}) - \Phi(0)]\}}{\int_{\text{WSC}} d^3 r \exp\{-\beta[\Phi(\mathbf{r}) - \Phi(0)]\}}. \end{aligned} \quad (\text{A.12})$$

Fig. 7 (left panel) shows the phase diagram of the Yoshida-Kamakura potential (3.12) for $a = 2.1$ as mapped out in the way just explained. A zoom on the low-pressure region of the phase diagram is presented in the right panel of Fig. 7. Compared to the exact phase diagram of Ref. [23], we see that the theory correctly accounts for the succession and extent of solid phases (with the unique omission of the cI16 solid), though still overestimating the values of the melting temperature by approximately 100% for all pressures. In the same picture, I also plotted the line encompassing the region of density anomaly as computed within the Mansoori-Canfield theory. The shape of this line compares well with that of the same line as obtained from simulation.

[*] E-mail: Santi.Prestipino@unime.it

[2] See A. Parola, D. Pini, and L. Reatto, *Mol. Phys.* **10**, 503 (2009) and references therein.

[3] See, for instance, J.-P. Hansen and I. R. McDonald, *Theory of Simple Liquids*, 3rd edition (Academic Press, 2006).

[4] See, for instance, D. Frenkel and B. Smit, *Understanding Molecular Simulation*, 2nd edition (Academic Press, 2002).

[5] See e.g. G. Malescio, F. Saija, and S. Prestipino, *J. Chem. Phys.* **129**, 241101 (2008); S. V. Buldyrev *et. al.*, *J. Phys.: Condens. Matter* **21**, 504106 (2009).

[6] A short presentation of the method has been given recently in Ref. [7].

[7] S. Prestipino, F. Saija, and G. Malescio, *J. Chem. Phys.* **133**, 144504 (2010).

- [8] See, for instance, T. H. K. Barron and M. L. Klein, *Proc. Phys. Soc.* **85**, 523 (1965); L. D. Landau and E. M. Lifshitz, *Theory of Elasticity* (Pergamon, 1975); D. C. Wallace, *Statistical Physics of Crystals and Liquids* (World Scientific, 2002); M. C. Rechtsman, F. H. Stillinger, and S. Torquato, *Phys. Rev. Lett.* **101**, 085501 (2008).
- [9] O. Farago and Y. Kantor, *Phys. Rev. E* **61**, 2478 (2000).
- [10] F. Saija, S. Prestipino, and P. V. Giaquinta, *J. Chem. Phys.* **124**, 244504 (2006).
- [11] S.-A. Cho, *Phys. Stat. Sol. B* **94**, K123 (1979).
- [12] See, for instance, E. A. Mastny and J. J. de Pablo, *J. Chem. Phys.* **127**, 104504 (2007).
- [13] G. Malescio, S. Prestipino, and F. Saija, *Mol. Phys.* (2011), DOI:10.1080/00268976.2011.609146.
- [14] I. Errea, B. Rousseau, and A. Bergara, *Phys. Rev. Lett.* **106**, 165501 (2011).
- [15] T. R. Koehler, *Phys. Rev. Lett.* **17**, 89 (1966); N. S. Gillis, N. R. Werthamer, and T. R. Koehler, *Phys. Rev.* **165**, 951 (1968); H. Fukujama and P. M. Platzmann, *Solid State Commun.* **15**, 677 (1974); P. M. Platzmann and H. Fukujama, *Phys. Rev. B* **10**, 3150 (1974); L. Pietronero and E. Tosatti, *Solid State Commun.* **32**, 255 (1979).
- [16] F. H. Stillinger, *J. Chem. Phys.* **65**, 3968 (1976).
- [17] A. Lang, C. N. Likos, M. Watzlawek, and H. Löwen, *J. Phys.: Condens. Matter* **12**, 5087 (2000).
- [18] S. Prestipino, F. Saija, and P. V. Giaquinta, *Phys. Rev. E* **71**, 050102(R) (2005).
- [19] See, for instance, D. C. Wallace, *Thermodynamics of Crystals* (Dover Publications, 1998).
- [20] G. A. Mansoori and F. B. Canfield, *J. Chem. Phys.* **51**, 4958 (1969).
- [21] S. Prestipino, F. Saija, and G. Malescio, *Soft Matter* **5**, 2795 (2009).
- [22] J. E. Lennard-Jones and A. F. Devonshire, *Proc. R. Soc. London, Ser. A*, **163**, 53 (1937).
- [23] F. Saija, S. Prestipino, and G. Malescio, *Phys. Rev. E* **80**, 031502 (2009).